CHAPTER 4

DENSITY FUNCTIONAL STUDY ON CATALYTIC ACTIVITY OF ANIONIC Au_2^- AND $Au\text{-}Ag^-$ DIMER FOR NITRIC OXIDE OXIDATION

In this chapter, we have carried out Density functional study to observe the catalytic property of anionic Au_2^- and $Au\text{-}Ag^-$ dimer towards the oxidation of nitric oxide (NO). The chapter consists of two sections.

In **section 4.1**, DFT is used to study the mechanistic details of NO oxidation promoted by anionic gold dimer. Here, we studied a full catalytic cycle producing two NO_2 molecules. The reaction is explored along three possible pathways. Our theoretical results show that anionic gold dimers present catalytic activity towards NO oxidation, as indicated by calculated low energy barriers and high exothermicities. The present results provide an understanding of the catalytic oxidation of NO by Au-cluster based catalyst. For the first time, we have presented a systematic study on the structure and energetic of various reaction intermediates involved in NO oxidation by Au_2^- clusters using DFT [Deka, R. C., Bhattacharjee, D., Chakrabartty, A. K. and Mishra, B. K. Catalytic oxidation of NO by Au_2^- dimers: a DFT study. *RSC Advances*, 4:5399-5404, 2014].

In **section 4.2**, we have performed DFT calculations to study the oxidation pathway of NO catalysed by anionic $Au\text{-}Ag^-$ dimer. During our investigations, we have considered two most plausible pathways of NO oxidation. Our results show that the anionic Au-

Ag⁻ dimer can effectively catalyze NO oxidation reaction. In Au-Ag⁻, the Au site is more active than the Ag site, and the calculated energy barrier values for the rate determining step of the Au-site catalytic reaction are remarkably lower than those for both the Ag-site catalytic reactions. The T1 diagnostic calculation suggests that the multi-reference character is not an issue for present study [Bhattacharjee, D., Mishra, B. K., Chakrabartty, A. K. and Deka, R. C. Catalytic activity of anionic Au–Ag dimer for nitric oxide oxidation: a DFT study. *New Journal of Chemistry*, 39:2209-2216, 2015].

# 4. 1 CATALYTIC OXIDATION OF NITRIC OXIDE BY Au_2^- DIMER

4.1.1 INTRODUCTION

The removal of oxides of carbon and nitrogen which are emitted mainly in automobile exhaust is a major challenge in catalysis research and is a subject of many investigations due to their contribution towards green house effect [1-3]. Therefore, understanding the adsorption mechanism, dissociation of oxygen, and oxidation of NO at molecular level is very important to design. As a new kind of catalyst to reduce air pollution, nano-sized gold clusters have attracted considerable interest recently from both industrial and scientific communities [4-7]. Experimental and theoretical studies have proved that free and supported nano-sized gold clusters can effectively catalyze CO, NO and H_2 oxidation reaction at low temperature [8,9]. Using density functional theory, Ding *et al.* [10] investigate the NO molecule adsorption on the gold clusters and observed a strong ability to adsorb NO molecule for the majority of gold cluster. When we consider the Au_2^-dimer, Hakkinen and his group already describe it both theoretically and experimentally as the smallest and effective catalyst for CO oxidation [9,11]. As Au_2^- promotes CO oxidation in the gas phase, it is both natural and promising to investigate the catalytic activity of Au_2^- towards NO oxidation as well.
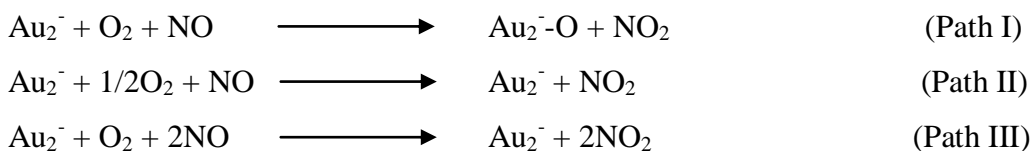
As per our knowledge, no detailed theoretical or experimental studies have been reported for this reaction. In view of the potential importance and the rather limited information, we carry out a detailed theoretical study on the PES of the title reaction using DFT to (1) provide the elaborate oxidation channels; (2) investigate the products of the title reaction to assist in further experimental identification; and (3) give deep insight into the mechanism of the reaction of gold anionic dimer with nitrogen oxide. Density functional theory (DFT) is already established as a valuable tool to study the properties of molecules and materials [12,13]for predicting reaction mechanisms. [14,15]. In this present study, for the first time, we have presented a systematic study on the structure and energetic of various reaction intermediates involved in NO oxidation by Au_2^- dimer.

4.1.2 COMPUTATIONAL DETAILS

The focus of our detail study is based on the following reaction:

$$2NO + O_2 \xrightarrow{Au_2^-} 2NO_2 \tag{4.1}$$
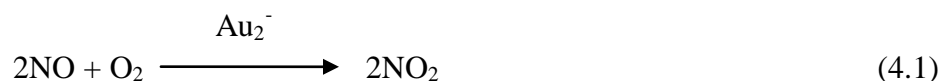
The three most plausible pathways for the oxidation of NO are investigated during present study as given by pathways (I-III) and shown in Scheme 1.

$$Au_2^- + O_2 + NO \longrightarrow Au_2^- \text{-} O + NO_2 \tag{Path I}$$

$$Au_2^- + 1/2 O_2 + NO \longrightarrow Au_2^- + NO_2 \tag{Path II}$$

$$Au_2^- + O_2 + 2NO \longrightarrow Au_2^- + 2NO_2 \tag{Path III}$$

We have performed all the calculations reported here, using the GAUSSIAN 09 suite of program [16]. In the framework of density functional theory (DFT), the hybrid B3LYP [17,18] functional is used to explore the stationary points on the potential energy surfaces. Considering the strong relativistic effect of Au, the Los Alamos LANL2DZ [19,20] Effective Core Pseudopotentials (ECP) and valence double-ζ basis sets for Au atoms is used. The C, N and O atoms are treated with the 6-311G(d,p) basis sets. No symmetric constraints are imposed during geometry optimization. In order to determine the nature of different stationary points on the potential energy surface, vibrational frequency calculations are also performed using the same level of theory at which the optimization was made. All the stationary points have been characterized as either minima (the number of imaginary frequencies NIMAG = 0) or transition structures (NIMAG = 1).

To ensure reliability of the reaction path, the connections between the transition state and the corresponding minima have been verified using an intrinsic reaction coordinate (IRC) calculations developed by Gonzalez and Schlegel in the mass-weighted internal coordinate system [21]. Previous investigations [22-24] showed that the B3LYP/LANL2DZ combinations are sufficiently accurate for describing noble-metal systems. The binding orientations of Au_2^- with NO and O_2 are studied by observing the HOMO and LUMO isosurfaces.
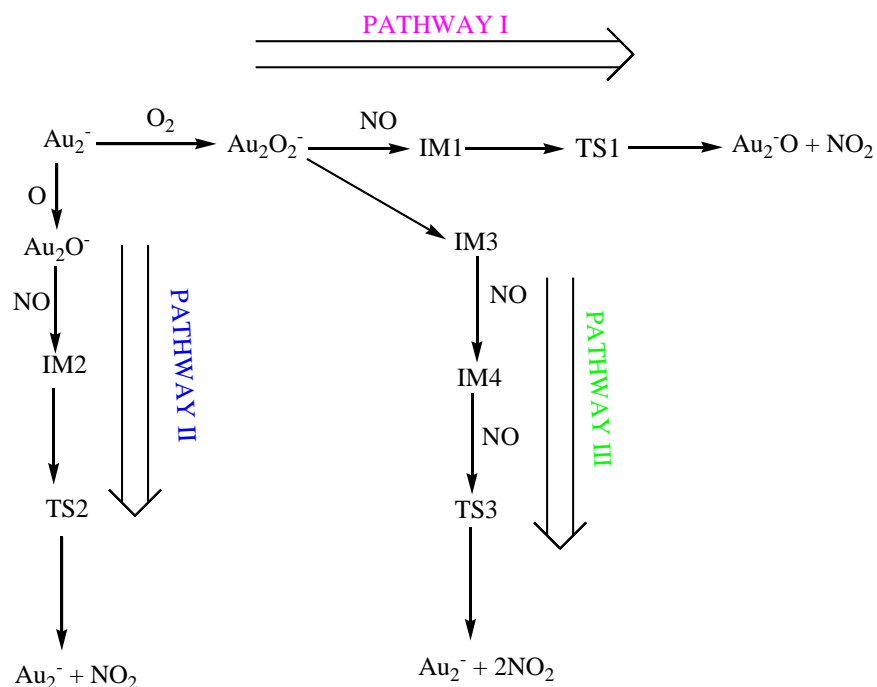
Scheme 4.1.1   Reaction Path ways for oxidation of NO to NO_2 by Au_2^- dimmer

The thermochemical parameters like standard reaction enthalpy (ΔH_r) and Gibbs free energy (ΔG_r) at a temperature T were estimated from the difference of H and G values of products and reactants at that temperature:

$$\Delta H_r(T) = \sum_{prod}(E_0 + H_{corr}) - \sum_{React}(E_0 + H_{corr}) \tag{4.1}$$

$$\Delta G_r(T) = \sum_{prod}(E_0 + G_{corr}) - \sum_{React}(E_0 + G_{corr}) \tag{4.2}$$

Where E_0 is the total electronic energy including ZPE and H_{corr} and G_{corr} are the factors to be added to E_0 for getting enthalpy and Gibbs free energy, respectively, at a temperature T for taking into account the contribution of translation, rotation and vibrational motion of a molecule.

The H_{corr} and G_{corr} are defined as:

$$H_{corr} = H_{trans} + H_{rot} + H_{vib} + RT \tag{4.3}$$

$G_{corr} = H_{corr} - TS_{total}$ (4.4)

Where entropy; $S_{total} = S_{trans} + S_{rot} + S_{vib} + S_{el}$

The thermal zero point energy correction (TZPE) is the thermal correction to the internal energy at 298 K and is given as a sum over four components for contributions from electronic, vibrational, rotational and translational degrees of freedom. The zero point vibrational energy ZPVE (or ZPE) results from the vibrational motion of molecular systems even at 0 K and is calculated for a harmonic oscillator model as a sum of contributions from all vibrational modes of the system. The heat of adsorption ($-\Delta H_{ads}$) is defined as:

$- H_{ads} = (E_{cluster} + H_{adsorbate}) - E_{cluster/adsorbate}$ (4.5)

Where, $E_{cluster/adsorbate}$, is the total energy of the adsorbate on the cluster, $E_{cluster}$ is the total energy of the bare cluster and $H_{adsorbate}$ is the enthalpy of the adsorbate.

4.1.3 RESULTS AND DISCUSSION

To clarify the reliability of our calculations, we have calculated the geometries and binding energies for Au_2^--O_2, Au_2^--CO, and Au_2^--NO. Our calculated values for binding energies of O_2, CO and NO over Au_2^- are 19.29, 7.16 and 16.50 kcal mol^{-1}, respectively. The binding energy of CO is in good agreement with the reported value of Liu *et al.* [25].

The values of thermodynamic calculations performed at DFT level for free energies, reaction enthalpies and entropies with thermal zero-point energy corrections (TZPE) associated with pathways (1-3) are listed in Table 4.1.1. Optimized geometries of reactants, intermediates, transition states and products obtained at the DFT level are shown in Figure 4.1.1. Transition states searched on the potential energy surfaces of pathways (I-III) are characterized as TS1, TS2 and TS3, respectively.

Table 4.1.1 Thermochemical data for the oxidation pathways of NO calculated at DFT level of theory with TZPE corrections.

Reaction channels	$_r\Delta G°$ (298K) (kcal mol^{-1})	$_r\Delta H°$ (298K) (kcal mol^{-1})	$\Delta S°$ (298K) (cal mol^{-1}K^{-1})
Pathway I	18.08	9.90	-33.29
Pathway II	-24.16	-22.79	-16.20
Pathway III	-48.32	-45.59	-32.40

The observed vibrational frequencies of the stationary points calculated at B3LYP level of theory are provided in Table 4.1.2. These results predict that the reactant and products have stable minima on their potential energy surface and signifies with the occurrence of only real vibrational frequencies. On the other hand, transition states are characterized by the occurrence of only one imaginary frequency obtained at 390i, 246i and 534i cm^{-1} for TS1, TS2 and TS3, respectively. Visualization of the imaginary frequencies gives a qualitative confirmation of the existence of transition states connecting reactants and products. Intrinsic reaction path calculations (IRC) have also been performed for each transition state. The IRC plots for transition states results that the transition state structure connects smoothly the reactant and the product sides. The energies of reactants, transition states and products obtained in the IRC calculations are in good agreement with the individually optimized values at B3LYP/LANL2DZ level of theory. It is clear from Figure 4.1.2 that the HOMO and LUMO isosurfaces of Au$_2^-$, O$_2$ and NO clearly match with shapes and symmetries. It further explains the binding orientations of NO with Au$_2^-$ similar to O$_2$.
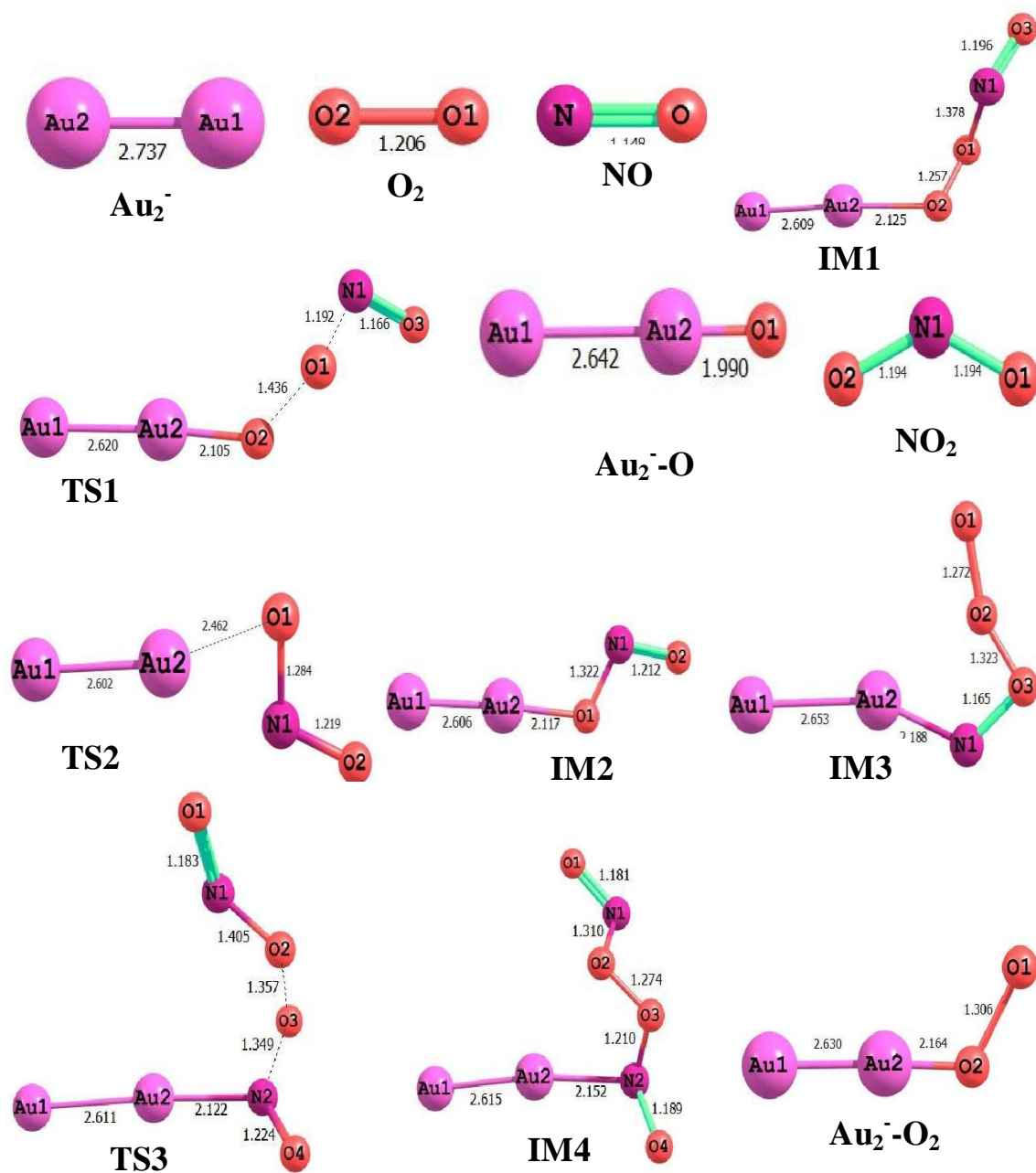
Figure 4.1.1 Optimized geometries of reactants, intermediates, transition states and products involved in the oxidative pathways of NO at B3LYP level.

Table 4.1.2 Harmonic vibrational frequencies of reactants, intermediates, transition states and products.

Species	Vibrational frequencies (cm^{-1})
Au_2^-	114
O_2	1641
Au_2^--O	119, 295, 296, 311
Au_2^--O_2	45, 60, 136, 216, 408, 1176
IM1	28, 56, 61, 137, 158, 228, 367, 465, 613, 808, 1006, 1647
IM2	12, 49, 137, 141, 185, 299, 820, 1067, 1557
IM3	42, 45, 73, 123, 132, 171, 172, 260, 379, 509, 1280, 1758
IM4	18, 30, 40, 47, 55, 68, 119, 139, 208, 231, 248, 437, 740, 825, 1329, 1499, 1647
TS1	390i, 27, 60, 88, 138, 191, 245, 435, 502, 728, 846, 1753
TS2	246i, 46, 57, 137, 141, 219, 785, 1223, 1505
TS3	534i, 27, 45, 53, 63, 138, 171, 176, 217, 242, 329, 397, 592, 638, 720, 953, 1453, 1699
NO	1988
NO_2	766, 1399, 1706

The initial step of NO oxidation is expected to be the complex formation of Au_2^- with O_2 and NO molecules. Path I start with the adsorption of O_2 on Au_2^- to form the superoxo like complex Au_2^--O_2. After the adsorption of O_2 on Au_2^--O_2, the coming NO attacks the adsorb O_2 to form a three species meta-stable complex IM1 which lies below the reactants by 39.31 kcal mol^{-1}. The NO then adsorbs O atom to produce an NO_2 via the transition state TS1. Calculated geometrical parameters of TS1 reveals that the O-O bond is weakening and the N-O bond is forming. Visualization of the optimized structure of TS1 further suggest the elongation of O-O bond (O1-O2) bond length from 1.257 to 1.436 Å (14%) and a simultaneous of the N-O (N1-O1) bond from 1.378 to 1.192 Å (13%). In the optimized geometry of TS1, NO abstracts an O atom to produce NO_2 and complete the cycle. Thermodynamic calculations reveal that this

pathway proceeds with an endothermicity of 9.90 kcal mol^{-1} along with an energy barrier of 16.18 kcal mol^{-1}. The calculated heat of adsorption for this path is found to be 48.33 kcal mol^{-1}.
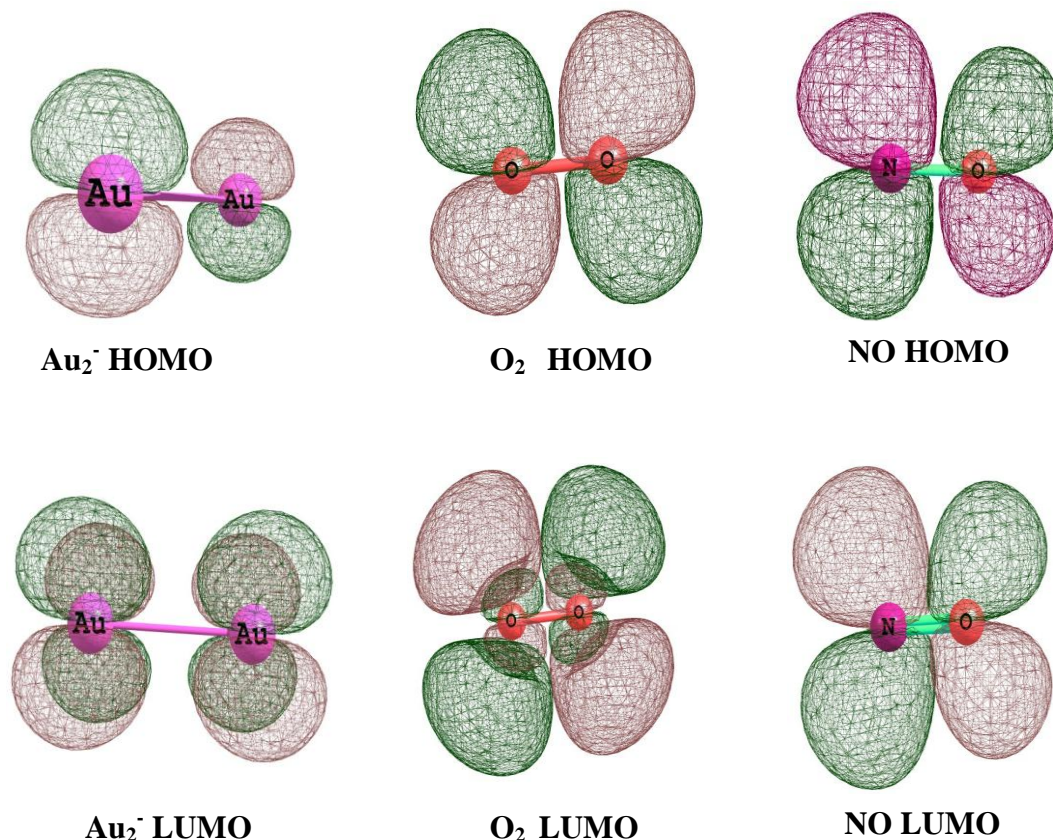

Au$_2$$^-$ HOMO   **O$_2$ HOMO**   **NO HOMO**

Au$_2$$^-$ LUMO   **O$_2$ LUMO**   **NO LUMO**

Figure 4.1.2 The HOMO and LUMO isosurfaces for Au$_2$$^-$ dimer, O$_2$, and NO molecules.

For Path II, initial complex of Au$_2$$^-$ with O and NO is denoted as IM2. From Table 4.1.1, we can see that Path II is exergonic ($\Delta G < 0$) and exothermic in nature. Hence it is thermodynamically facile. The heat of adsorption for this pathway is found to be 128.97 kcal mol^{-1}. The complex IM2 is stable by 58.59 kcal mol^{-1} than the reactants. The transition state involved along this path is TS2, where the transition vector related to the imaginary frequency of 246 cm^{-1} giving rise to the formation of product-like intermediate IM2. The barrier along this path is calculated to be 11.91 kcal mol^{-1}. The geometrical parameters of TS2 indicate that the Au-O bond is weakening

and the O-N bond is forming. The Au-O (Au2-O1) bond length elongates from 2.164 to 2.462 Å resulting in an increase of about 14%.

The stronger interaction of Au clusters with NO (with binding energy of 16.50 kcal mol^{-1}) forced us to explored another reaction channel (Path III) which involves a O-N-O-O-N-O group with the participation of two NO molecules. From Table 4.1.1, the ΔG_r value for this Pathway is found to be significantly negative at 298 K. Hence, it should be a spontaneous process at lower temperatures. Interestingly, ΔH_r and ΔG_r values indicate that this pathway should be thermodynamically more favored pathways. Path III involves the simultaneous formation of two NO_2 molecules with heat of adsorption value of 164.24 kcal mol^{-1}. Similar to Path I, by attaching the first NO molecule to IM1 we locate another meta-stable complex IM3 which lies below the reactants by 53.76 kcal mol^{-1}. Further attachment of second NO molecule to IM3 results IM4. Visualization of IM4 reveals that N atom binds to Au_2^- and associate one O of O_2 to form O-N-O-O-N-O group which lies below the reactants by 43.58 kcal mol^{-1} with simultaneous formation of two NO_2 molecules via TS3 with a barrier of 8.92 kcal mol^{-1}.

We have also constructed a schematic potential energy surface of the titled reaction obtained at the B3LYP + ZPE level as shown in Figure 4.1.3. In the construction of energy diagram, zero-point corrected total energies of the species are utilized. These energies are plotted with respect to the ground state energy of Au_2^- +O_2/O arbitrarily taken as zero. Figure 4.1.3, clearly indicates that Path III (O-N-O-O-N-O group) is the dominant path having lower barrier height for the NO oxidation promoted by Au_2^- dimer. Our calculated barrier heights for all the plausible pathways are comparable with the barrier height calculated by Liu *et al.* [25] for CO oxidation promoted by Au_2^- dimer.
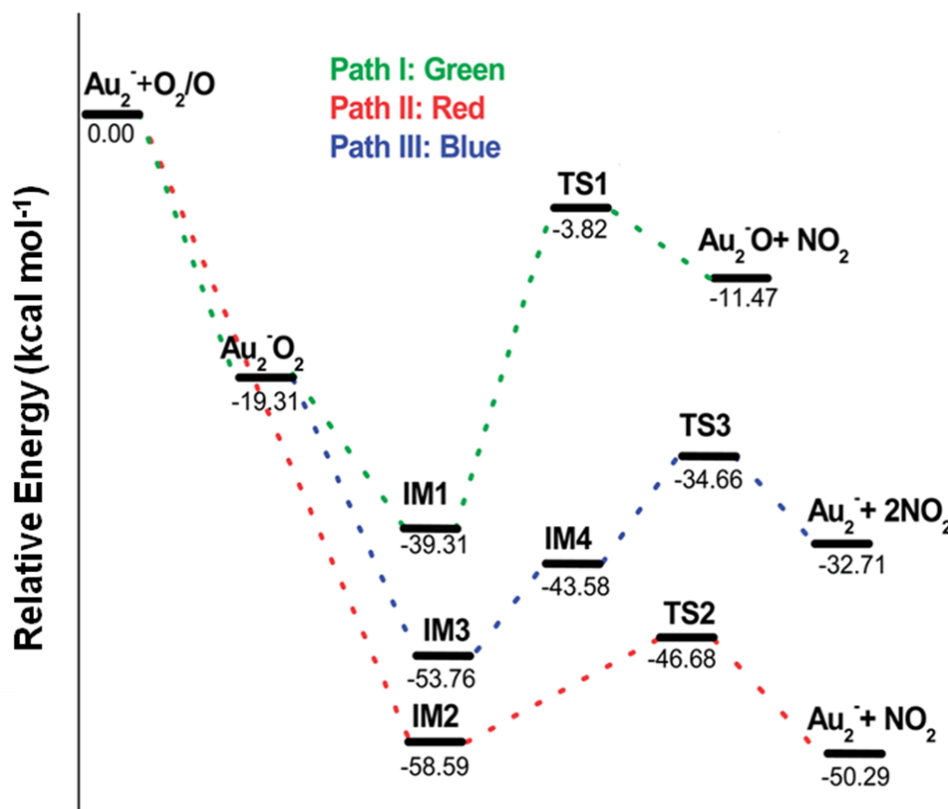
Figure 4.1.3 Potential energy profile of the NO oxidation by the Au_2^- dimer. The relative energies (in kcal mol^{-1}) were calculated with the ZPE corrections at the B3LYP/LANL2DZ level.

4.1.4 SALIENT OBSERVATIONS

We have presented here the potential energy profile (including geometries, energies and vibrational frequencies of reactant, intermediates, transition states and products) and thermochemical data for the oxidation of NO to NO_2 promoted by gold anionic dimer investigated at the DFT level of theory. The main observations results in this study are:

1. Au_2^- dimer shows catalytic activity towards NO oxidation.
2. HOMO and LUMO isosurfaces of Au_2^-, O_2, and NO have similar shapes and symmetries.

3. The energies of reactants, transition states and products obtained in the IRC calculations are in excellent agreement with the individually optimized values at B3LYP/LANL2DZ level of theory.

4. Energetic calculation reveals that the most dominant oxidation pathway is the Path III with lowest energy barrier for NO oxidation.

5. These theoretical studies can provide useful information on the reaction mechanism and can provide powerful guidelines for future experimental studies for the title reaction.

## 4.2 CATALYTIC ACTIVITY OF Au-Ag⁻ FOR NO OXIDATION

4.2.1 INTRODUCTION

Precious metals such as Au, Ag, Pd and Pt show potential catalytic activity towards the removal of poisonous green house gases like CO and NO [9,13,26]. The bimetallic clusters of these metals such as Au-Ag are much more promising than the monometallic ones because of their synergistic effects. They show novel catalytic behavior based on the effect of second metal element added [27]. The DFT calculation by Peng *et al.* [28] investigate the CO and O_2 adsorption as well as CO oxidation on the Au_mPd_n (m + n = 2–6) bimetallic clusters. They found that the adsorption energies of both CO and O_2 on Au_mPd_n (m + n = 2–6) are greater than those on the pure gold clusters of corresponding sizes, and unexpectedly greater than those on Pd clusters in some cases. Considering the catalytic activity of Au_2^- dimer towards CO oxidation as well as the enhance activity of bimetallic clusters, Liu *et al.* [25] studied the same reaction catalyzed by Au-Ag⁻ dimer in the gas phase and compared it with the pure Au_2^- dimer. They reveal that anionic Au-Ag⁻ dimer has great catalytic activity for CO oxidation and also the activity is higher compared to that of pure Au_2^- dimer. As Au-Ag⁻ promotes CO oxidation in the gas phase; it is quite obvious for us to investigate the catalytic activity of Au-Ag⁻ towards NO oxidation. Therefore, in this work, we have investigated the catalytic activity of Au-Ag⁻ dimer towards NO oxidation. Since gold is the most electronegative metal and it also shows the polarization effect, its alloy nanoparticles supported on substrates leads to the negatively charged nanoparticles. Thus the anionic clusters are suitable for mimicking the catalytic reactivities of Au and Au-Ag nanoparticles.Thus the anionic clusters are appropriate for mimicking the catalytic reactivities of Au and Au-Ag nanoparticles. By virtue of potential significance and finite information, we have carried out a detailed Density Functional calculation with the objectives: (1) to provide the elaborate oxidation channels; (2) investigate the products of the title reaction to assist in further experimental identification; and (3) to provide deep insight into the mechanism of the reaction of anionic gold-silver dimer with nitrogen oxide.

4.2.2 COMPUTATIONAL DETAILS

The aim of our detail study was based on the following reaction.

$$2NO + O_2 \xrightarrow{\text{Au-Ag}^-} 2NO_2 \qquad (4.2)$$
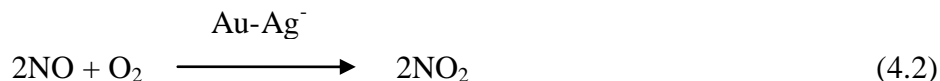
For Au-Ag- dimer, the reaction branches into the Au-site and Ag-site catalytic series. We have investigated two most plausible pathways for the oxidation of NO during present study as given by path 1 and path 2.
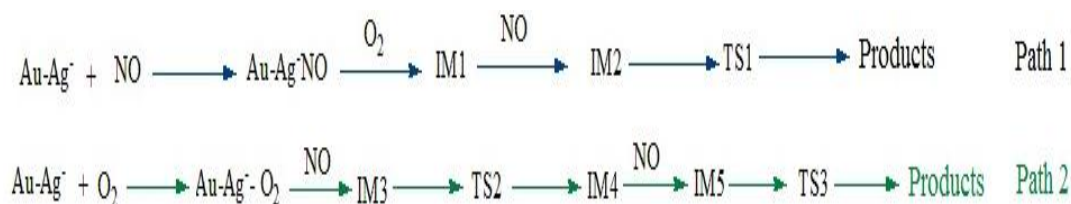
Where, IM and TS represents intermediate and transition states, respectively. The computational method is almost same as the previous section. All the calculations are performed using Gaussian 09 suits of program [12] In the frame work of density functional theory (DFT), we employ the hybrid B3LYP [17,18] functional to explore the stationary points on the potential energy surfaces. Considering the strong relativistic effect of Au and Ag, we have used the Los Alamos LANL2DZ [19,20] basis set. The N and O atoms are treated with the 6-311G+(d) basis sets. No symmetric constraints are imposed during geometry optimization. For fair determination of the nature of different stationary points on the potential energy surface and to consider the zero-point vibrational energies (ZPEs), vibrational frequency calculations are also performed using the same level of theory at which the optimization was made. All the stationary points have been characterized as either minima (the number of imaginary frequencies NIMAG = 0) or transition structures (NIMAG = 1). To ensure reliability of the reaction path, intrinsic reaction coordinate (IRC) calculations are employed. The binding orientations of Au-Ag$^-$ with NO and O_2 were studied by observing the HOMO and LUMO isosurfaces. The thermochemical parameters like standard reaction enthalpy (ΔH_r) and Gibbs free energy (ΔG_r) at a temperature T are also estimated from the difference of H and G values of products and reactants at that temperature using the same formulas as provided in section 4.1.

4.2.3 RESULTS AND DISCUSSION

B3LYP functional is sufficiently accurate for describing noble-metal systems as reported in the previous studies [25, 29-31]. To further check the reliability of our methods, we have calculated the bond lengths for Au-Ag$^-$, NO and O_2 and dissociation energy calculations for Au-Ag$^-$ and NO and compare them with corresponding experimental values. As shown in Table 4.2.1, our calculated values at B3LYP level for bond lengths and dissociation energies are in a reasonable agreement with the corresponding experimental results [24,32,33]. To check the additional accuracy for interaction of NO and O_2 with the metal species, we have also compared the bond lengths and dissociation energies for AgO, AuO and AgN with the previous results [33-36]. These results are also found to be in good agreement with the previously reported data as provide in Table 4.21. Therefore, we come to the conclusion that the level of theory selected in our study can accurately and precisely describe the systems.

Table 4.2.1: Calculated and experimental bond lengths, d (in Å) and dissociation energies, D.E.in eV) at B3LYP level

Methods	**d (Å)**			**D.E. (eV)**		
	Au-Ag$^-$	O_2	NO	Au-Ag	O_2	
B3LYP	2.771	1.206	1.148	1.81	5.29	
Exp.	2.772[a]	1.209[b]	1.151[c]	2.08±0.1[a]	5.12[c]	
	AgO	AuO	AgN	AgO	AuO	AgN
B3LYP	2.074	1.924	2.214	1.49	1.45	1.44
Exp.	2.0[c]	1.96-1.99[d]	2.11[e]	2.21±0.21[f]	2.23±0.21[f]	

[a]Ref. [32], [b]Ref. [31], [c]Ref. [33], [d]Ref. [34], [e]Ref. [35], [f]Ref. [36]

In order to access the multi-reference characteristics, we have performed the T1 diagnostic [37] at CCSD(T) level of theory for transition states and results are given in Table 4.2.2. The table shows that the calculated T1 diagnostic values are considerably lower than 0.045. It has been established that a T1 value larger than 0.045 indicates a significant multi-reference character [38]. Therefore, the transition states reported in this work do not possess a multi-reference character. The thermochemical studies have been performed to analyze the stability of all the species involved in the reactions. The ΔH_r value obtained is-2.87 eV at 298 K indicating the exothermicity of the reaction. The calculated free energy (ΔG_r) value of -3.07 eV reveals that the reaction is spontaneous in nature.

Table 4.2.2 T1 diagnostic values of the transition states for Ag and Ag sites of Au-Ag⁻ -dimer using B3LYP functional.

	TS1	TS2	TS3
Ag site	0.032	0.025	0.023
	TS4	TS5	TS6
Au site	0.029	0.026	0.024

4.2.3.1 Complexes of Au-Ag⁻ with O_2 and NO

The formation of complexes between Au-Ag⁻ with O_2 and NO are shown in Figure 4.2.1. In these calculations, various possible geometries where the O_2 and NO molecules approach the dimer with different orientations as well as different possible spin combinations between the dimer with O_2 and NO molecule are considered. The most stable structures are shown in Figure 4.2.1. For O_2 adsorption (Table 4.2.3), the other two possible orientations leading to dissociative adsorption are found to be less favorable energetically having lower values of binding energies. Similarly, for NO adsorption also, we optimized one additional orientation by combining N atom together with both Au and Ag atoms. But this structure possessed binding energy value 0.08 eV

only which is much smaller compared to the side bonded orientation. The less favorable orientations are not considered during the present study.
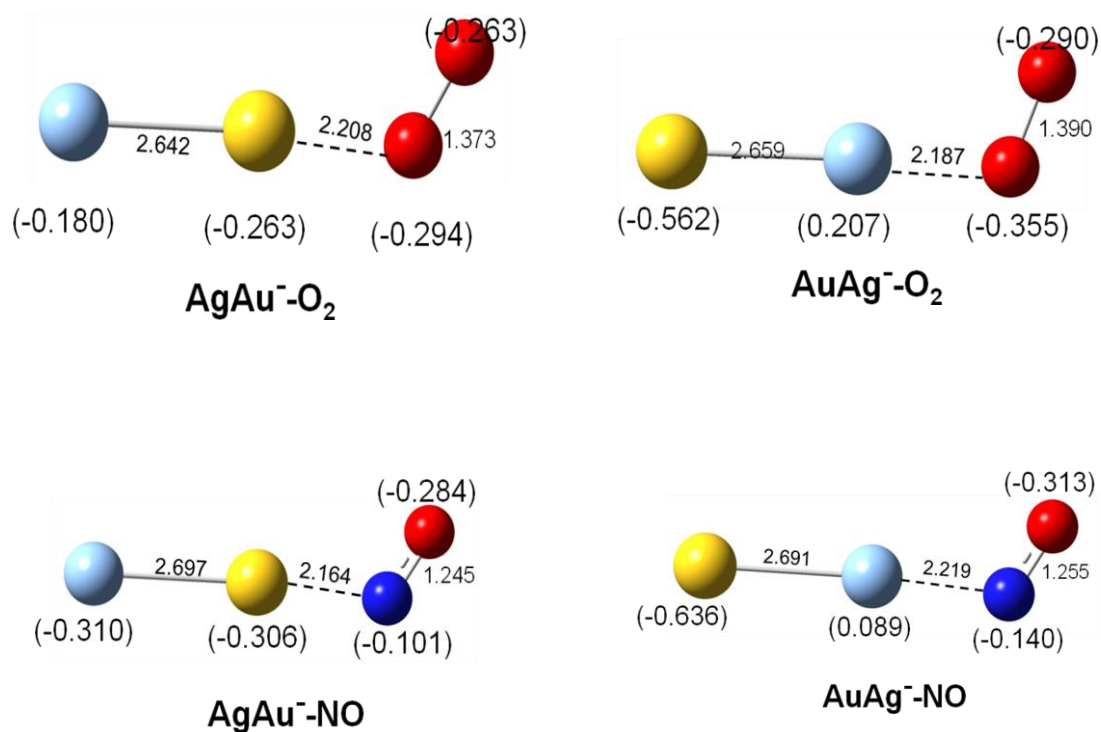

Figure 4.2.1 Optimized geometries for complexes between O_2 and NO molecules with Au-Ag- dimers in two different sites. The numbers in parentheses are calculated natural charges of atoms (in e). (Gold in yellow, Ag in sky blue, oxygen in red and nitrogen in dark blue colors)

The preferred orientations are identical with that of O_2 and CO binding to Au_2^- dimer as reported earlier [39]. Following the previous catalytic studies of our group, [13,40] for the catalyst Au-Ag⁻, we have checked the stable structure by varying the spin multiplicity and found that the doublet system is most stable. The energies for the quartet and sextet structures are quite high compared to doublet structures as reported in Table 4.2.4. Therefore, we have considered the doublet Au-Ag⁻ structure for the whole reaction.

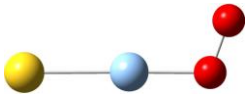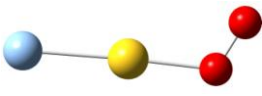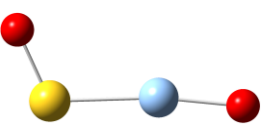**Table 4.2.3** Binding energies for different binding orientations of O_2 and NO with Au-Ag⁻ dimer
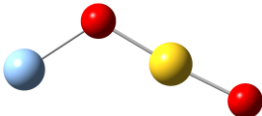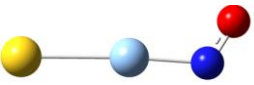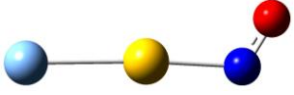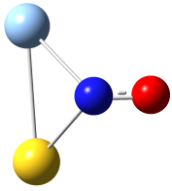
Structure	Binding Energy (in eV)
	1.73
	1.16
	0.03
	1.14
	0.77
	0.56
	0.08

Table 4.2.4 Relative energies of different species with various spin multiplicities.

AuAg⁻		AuAg⁻NO		AuAg⁻O$_2$	
Multiplicity, S	Relative Energy (in eV)	Multiplicity, S	Relative Energy (in eV)	Multiplicity, S	Relative Energy (in eV)
2	0.00	1	0.00	2	0.00
4	2.09	3	0.21	4	2.35
6	7.91				

For Au-Ag⁻ dimer, O$_2$ can bind to Ag or Au site, forming complex AuAg⁻-O$_2$ or AgAu⁻-O$_2$. The calculated binding energies are 1.733 and 1.162 eV for these two complexes, respectively. This indicates that O$_2$ preferably binds to Ag-site of AuAg⁻ similar to the previous study [25]. This fact was further supported by calculated longer O-O distance (1.390 Å) in AuAg⁻-O$_2$ than that in AgAu⁻-O$_2$ (1.373 Å) which are in close agreement with previous reported values [25]. The amount of electron transfer from the dimer to O$_2$ in these two complexes is 0.645 e in AuAg⁻-O$_2$ and 0.557 e in AgAu⁻-O$_2$. The transferred electrons enter the π* orbital of O$_2$ to reduce O-O bond strength. More the electrons are transferred; the larger will be the O-O distances in AuAg⁻-O$_2$. Similarly, for the complexes of AuAg⁻ with NO, our calculations show that the binding energies of NO over the Ag and Au sites are 0.775 and 0.562 eV, respectively. This reveals that the Ag-site of AuAg⁻ is also more active toward NO binding than the Au-site. For binding of O$_2$ and NO with AuAg⁻ too, we have considered different spin multiplicities (Table 4.2.4) and choose the most stable one for this study. On comparing the relative stability of the complexes of AuAg⁻ with O$_2$ to those with NO, we see that the interaction of AuAg⁻ with O$_2$ is stronger than that with NO. This is also confirmed by the geometrical parameters shown in Figure 4.2.1. From the figure, it can be seen that the O-O distance in AuAg⁻-O$_2$ is increased by 14.9% compared to that in isolated O$_2$, while the N-O distance in AuAg⁻-NO is only

increased by 9.0% compared to that in isolated NO, indicating a stronger interaction of AuAg$^-$ with O_2 than with NO. It is also clear from Figure 4.2.2 that the HOMO and LUMO isosurfaces of Au-Ag$^-$, O_2, and NO clearly match with shapes and symmetries. It further explains the binding orientations of NO with Au-Ag$^-$ similar to O_2.
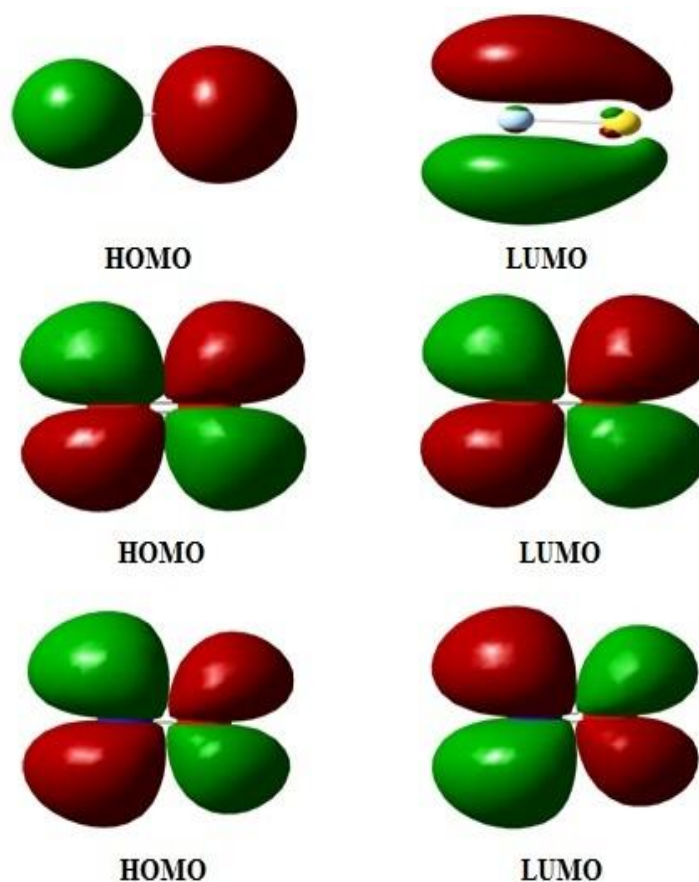

Figure 4.2.2 HOMO and LUMO isosurfaces for Au-Ag$^-$ dimer, O_2 and NO molecules.

4.3.3.2 NO oxidation along Ag sites of Au-Ag$^-$ dimer

Optimized geometries of reactants, intermediates, transition states and products obtained at the DFT level using B3LYP functional are shown in Figure 4.2.3 for both Ag and Au sites. Transition states searched on the potential energy surfaces of pathways (I-II) are characterized as TS1, TS2 and TS3, respectively. This search was made along the minimum energy path on a relaxed potential energy surface.

The formation of complexes of Au-Ag$^-$ with O$_2$ and NO molecules is expected to be the initial step of NO oxidation. Path I start with the adsorption of NO with the Au-Ag$^-$ dimer. After this adsorption, the attack of upcoming O$_2$ molecules gives IM1 which lies below the reactant by 2.24 eV. Subsequently, another NO molecule attacks IM1 to give IM2 which involves with O-N-O-O-N-O like species. From IM2, we get two NO$_2$ molecules simultaneously via TS1 involving a O-N-O-O-N-O group (Figure 4.2.3). Calculated geometrical parameters of TS1 clearly indicate that the O-O bond is weakening and the N-O bond is forming. Visualization of the optimized structure of TS1 reveals the elongation of O-O bond length from 1.506 to 1.573 Å with a simultaneous shrinkage of the N-O bond from 1.292 to 1.242 Å. In the optimized geometry of TS1, NO abstracts an O atom to produce NO$_2$ and thus complete the cycle. The TS1 confirms its existence with an imaginary frequency of 568i cm^{-1}. All other structures associated with only positive vibrational frequencies.

For pathway II, the initial step is the adsorption of O$_2$ molecule with Au-Ag$^-$ to give a preadsorbed superoxo like species Au-Ag$^-$-O$_2$. The first NO molecule then attack this species to give IM3 which lies below the reactants by 2.67 eV. From IM3, we get IM4 via TS2 (Figure 4.2.3) which involves a O-O-N-O group and associated with an imaginary frequency of 396i cm^{-1}. In this step one NO$_2$ molecule is released. The attack of second NO molecule on IM4 results IM5. From IM5, second NO$_2$ molecule is released via TS3 which possesses an imaginary frequency of 140i cm^{-1}. Calculated geometrical parameters of TS2 and TS3 indicate that the O-O and Ag-O bonds are weakening and the O-N bond is forming.
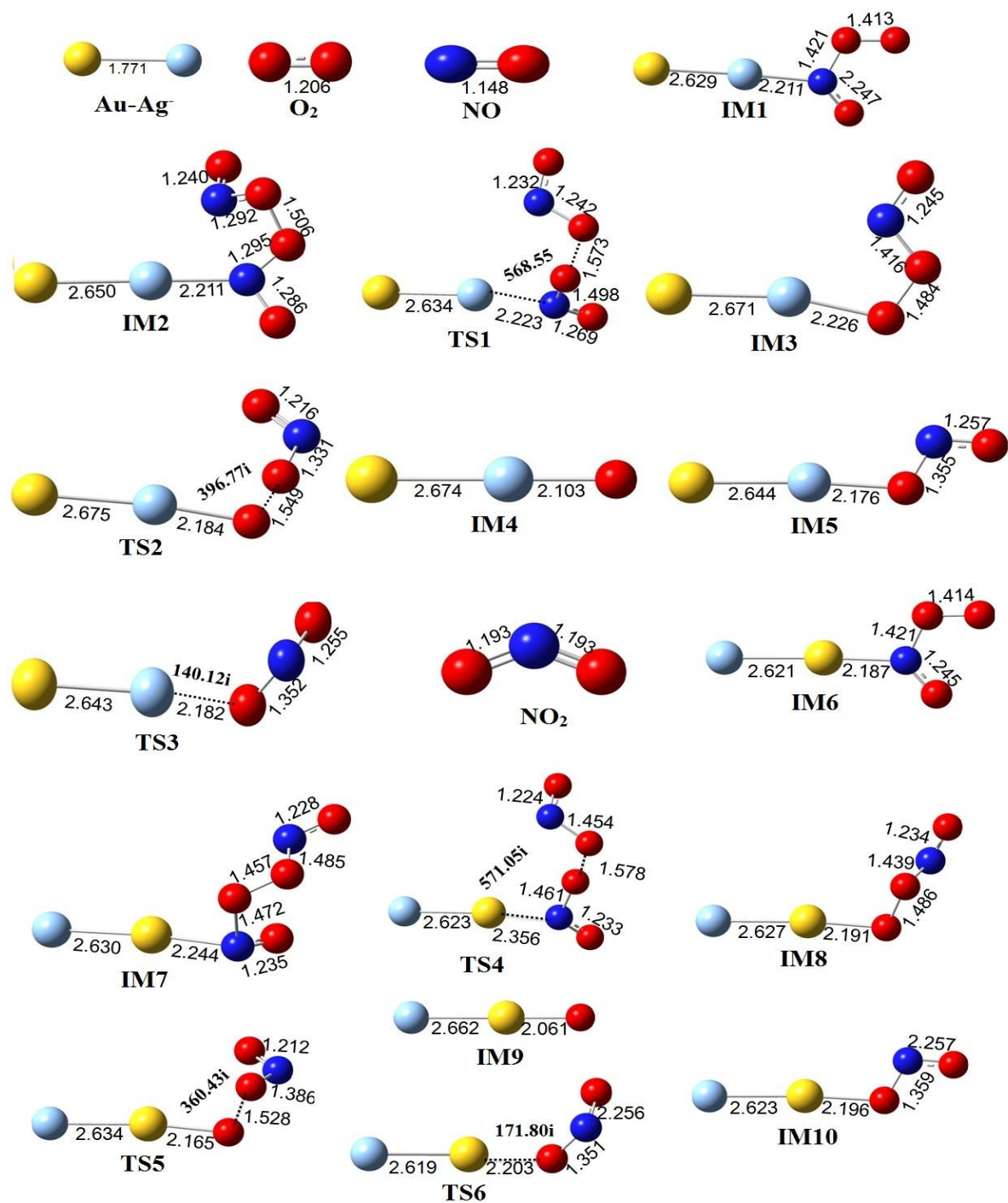
Figure 4.2.3 Optimized geometries of reactants, intermediates, transition states and products involved in the oxidative pathways of NO by Au-Ag⁻ dimer along Ag and Au sites. (Gold in yellow, Ag in sky blue, oxygen in red and nitrogen in dark blue colors, 'i' represents imaginary frequency)

Similar analysis made on the optimized structure of TS2 and TS3 reveals that in TS2, of O-O bond lengths elongates from 1.484 to 1.549 Å and of N-O bond lengths shrinkages from 1.416 to 1.331 Å. Similarly, TS3 involves elongation of Ag-O bond length from 2.176 to 2.182 Å and shrinkage of N-O bond lengths from 1.355 to 1.352 Å. To verify the formation of transition states, we have calculated the IRC paths for both the pathways. The IRC plots for transition states reveal that the transition state structures connect smoothly the reactant and the product sides. The energies of reactants, transition states and products obtained in the IRC calculations are in excellent agreement with the individually optimized values at the B3LYP/LANL2DZ level of theory.
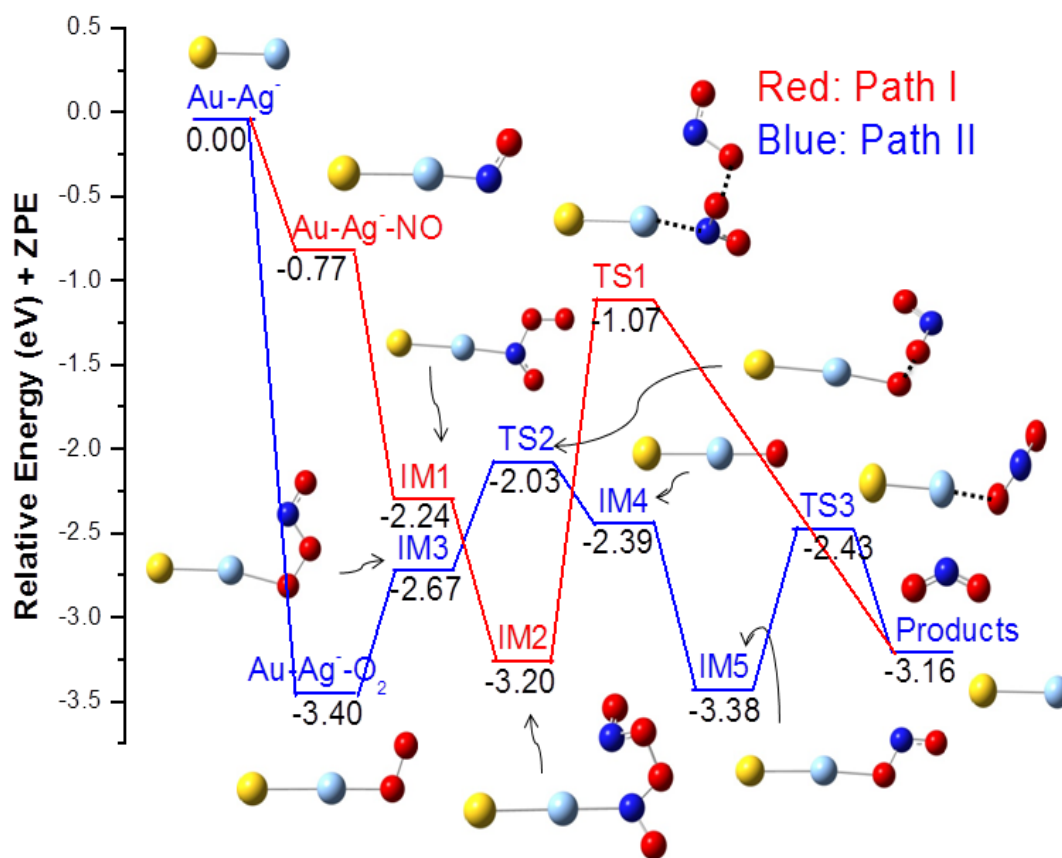

Figure 4.2.4 Relative energy profile for the NO oxidation by Au-Ag⁻ dimer along Ag site

We have also constructed schematic potential energy surfaces of the titled reaction obtained for both the pathways at the B3LYP + ZPE levels to search the most dominant path of the reaction (Figure 4.2.4) In the construction of energy diagram, zero-point corrected total energies are utilized. These energies are plotted with respect to the ground state energy of reactants (Au-Ag$^-$ +O_2/NO) arbitrarily taken as zero. From Figure 4.2.4, it is clear that Pathway II is the dominant path involving lower barrier height for the NO oxidation promoted by Au-Ag$^-$ dimer. The barrier heights obtained from the energy profile diagrams are listed in Table 4.2.5.

Table 4.2.5 Calculated barrier heights for both pathways along Ag and Au sites of Au-Ag$^-$-dimer at B3LYP level.

Reaction Sites	Energy Barriers (eV)		
	Pathway I	Pathway II	
Ag site	2.13	1.37	0.95
Au site	1.68	1.41	0.17

4.2.3.3 NO oxidation along Au sites of Au-Ag- dimer

The two reaction pathways are carried out for the Au sites of Au-Ag$^-$ dimer as well. The energy profile diagram for Au site is shown in Figure 4.2.5. For pathway I, TS4 involves with an imaginary frequency of 571i cm^{-1}. Visualization of the optimized structure of TS4 reveals the elongation of O-O bond length from 1.457 to 1.578 Å with a simultaneous shrinkage of the N-O bond from 1.485 to 1.454 Å. In the optimized geometry of TS4, NO abstracts an O atom to produce NO_2 and complete the cycle. The barrier height for this pathway is found to be 1.68 eV.
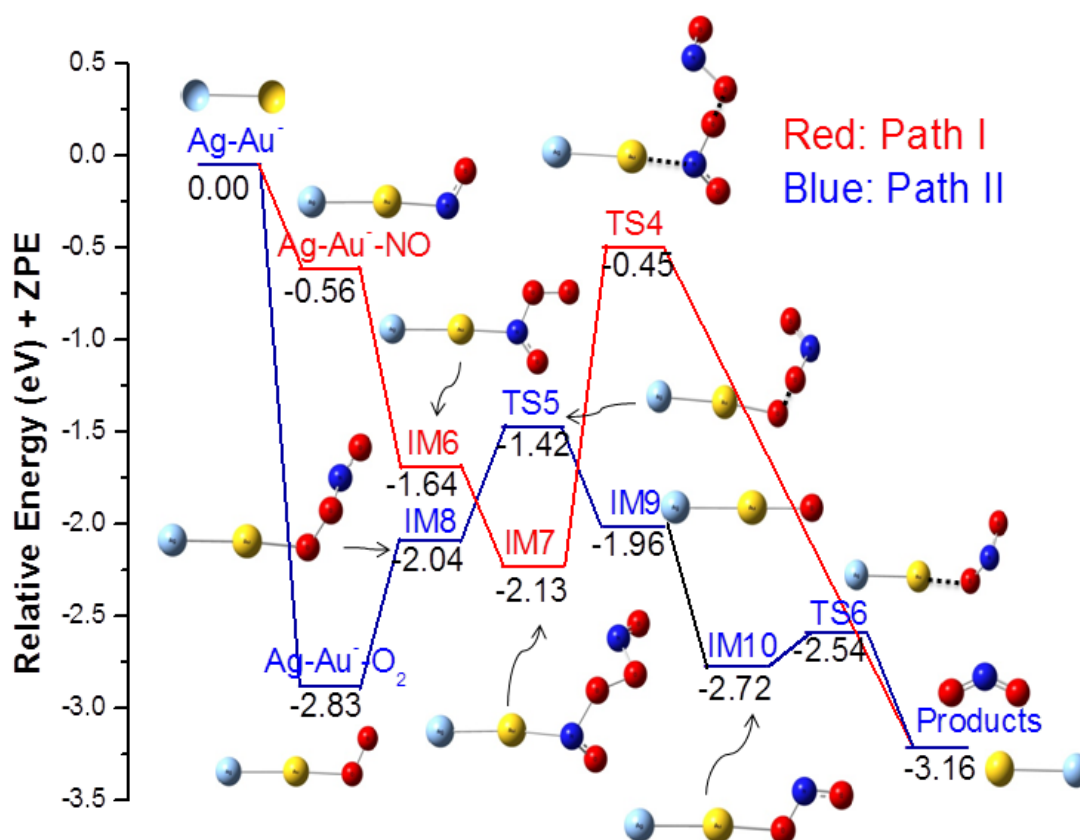
Figure 4.2.5 Relative energy profile for the NO oxidation by Au-Ag$^-$ dimer along Au site.

Similarly for pathway II, TS5 and TS6 are associated with imaginary frequencies of 360i cm^{-1} and 171i cm^{-1}, respectively. Calculated geometrical parameters of TS5 and TS6 indicate that the O-O and Au-O bond are weakening and the O-N bond is forming. Similar analysis made on the optimized structure of TS5 and TS6 reveals the elongation of O-O bond length from 1.486 to 1.528 Å and shrinkage of N-O bond length from 1.439 to 1.386 Å in case of TS5 and elongation of Au-O bond length from 2.196 to 2.203 Å and shrinkage of N-O bond length from 1.359 to 1.351 Å in case of TS6, respectively. The barrier heights obtained from the energy profile diagram are shown in Table 4.2.5. Here also, we have calculated the IRC paths for both the pathways to verify the formation of TS. The IRC plots for transition states reveal that the transition state structure connects smoothly the reactant and the product sides.

The energies of reactants, transition states and products obtained in the IRC calculations are in excellent agreement with the individually optimized values.

From the above results, we can see that for both Au and Ag sites of Au-Ag$^-$-dimer, pathway II is more dominant compared to pathway I as indicated by its lower barrier height in both the cases. However, when we compare the reactions in both the sites, it clearly indicates the preference of Au site compared to Ag site for NO oxidation (from the comparison of energy barriers of Table 4.2.5) in Au-Ag$^-$-dimer. This is in accordance with the previous report [25] that the Au site is more active than the Ag site for AuAg$^-$ dimer towards CO oxidation.

4.2.4 SALIENT OBSERVATIONS

We have presented here a systematic study on oxidation of NO to NO$_2$ promoted by gold-silver anionic dimer investigated at the DFT level of theory. The study reveals the following observations:

1. Au-Ag$^-$ dimer shows remarkable catalytic activity towards NO oxidation.
2. Thermodynamic calculations suggest that the reaction is exothermic and spontaneous.
3. HOMO and LUMO isosurfaces of Au-Ag$^-$, O$_2$, and NO clearly match with shapes and symmetries.
4. Energetic calculation reveals that the most dominant oxidation pathway is the Path II for NO oxidation involving O-O-N-O group.
5. For Au-Ag$^-$ dimer, the Au site is more active than the Ag site as indicated by lower calculated energy barrier values.

BIBLIOGRAPHY

[1] Granger, P., Dujardin, C., Paul, J. F. and Leclercq, G. An overview of kinetic and spectroscopic investigations on three-way catalysts: mechanistic aspects of the CO+ NO and CO+ N_2O reactions. *Journal of Molecular Catalysis A: Chemical*, 228:241-253, 2005.

[2] Silverston, P.L. Automotive exhaust catalysis under periodic operation. *Catalysis Today,* 25:175-195, 1995.

[3] Pârvulescu, V. I., Grange, P. and Delmon, B. Catalytic removal of NO. *Catalysis Today*, 46(4):233-316, 1998.

[4] Bond, G. C. and Thompson, D. T. Gold catalysis. *Catal Rev-Sci Eng,* 41:319-388, 1999.

[5] Okumura, M., Nakamura, S., Tsubota, S., Nakamura, T., Azuma, M. and Haruta, M. Chemical vapor deposition of gold on Al_2O_3, SiO_2, and TiO_2 for the oxidation of CO and of H_2. *Catalysis Letters*, 51(1):53-58, 1998.

[6] Valden, M., Lai, X. and Goodman, D. W. Onset of catalytic activity of gold clusters on titania with the appearance of nonmetallic properties. *Science*, 281(5383):1647-1650, 1998.

[7] Haruta, M. When gold is not noble: catalysis by nanoparticles. *The Chemical Record*, 3(2):75-87, 2003.

[8] Lopez, N. and Nørskov, J. K. Catalytic CO oxidation by a gold nanoparticle: a density functional study. *Journal of the American Chemical Society*, 124(38):11262-11263, 2002.

[9] Ha¨kkinen, H. and Landman, U. Gas-Phase catalytic oxidation of CO by Au_2^-. *Journal of the American Chemical Society*, 123:9704-9705, 2001.

[10] Ding, X., Li, Z., Yang, J., Hou, J. G. and Zhu, Q. Theoretical study of nitric oxide adsorption on Au clusters. *The Journal of Chemical Physics*, 121(6):2558-2562, 2004.

[11] Socaciu, L. D., Hagen, J., Bernhardt, T. M., Wöste, L., Heiz, U., Häkkinen, H. and Landman, U. Catalytic CO oxidation by free Au_2^-: experiment and theory. *Journal of the American Chemical Society*, 125(34):10437-10445, 2003.

[12] Stamenkovic, V., Mun, B. S., Mayrhofer, K. J., Ross, P. N., Markovic, N. M., Rossmeisl, J., Greeley, J. and Nørskov, J. K. (2006). Changing the activity of electrocatalysts for oxygen reduction by tuning the surface electronic structure. *Angewandte Chemie*, 118(18):2963-2967, 2006

[13] Kalita, B. and Deka, R. C. Reaction intermediates of CO oxidation on gas phase Pd_4 clusters: a density functional study, *Journal of the American Chemical Society*. 131(37):13252--13254, 2009.

[14] Valero, R., Gomes, J. R., Truhlar, D. G. and Illas, F. Density functional study of CO and NO adsorption on Ni-doped MgO (100). *The Journal of Chemical Physics*, 132(10):104701, 2010.

[15] Song, W. and Hensen, E. J. A computational DFT study of CO oxidation on a Au nanorod supported on CeO_2(110): on the role of the support termination. *Catalysis Science and Technology*, 3(11):3020-3029, 2013.

[16] Frisch, M.J., Trucks, G.W., Schlegel, H.B., Scuseria, G.E., Robb, M.A., Cheeseman, J.R., Scalmani, G., Barone, V., Mennucci, B., Petersson, G.A., Nakatsuji, H., Caricato, M., Li, X., Hratchian, H.P., Izmaylov, A.F., Bloino, J., Zheng, G., Sonnenberg, J.L., Hada, M., Ehara, M., Toyota, K., Fukuda, R., Hasegawa, J., Ishida, M., Nakajima, T., Honda, Y., Kitao, O., Nakai, H., Vreven, T., Montgomery, J.A., Jr., Peralta, J.E., Ogliaro, F., Bearpark, M., Heyd, J.J., Brothers, E., Kudin, K.N., Staroverov, V.N., Kobayashi, R., Normand, J., Raghavachari, K., Rendell, A., Burant, J.C., Iyengar, S.S., Tomasi, J., Cossi, M., Rega, N., Millam, J.M., Klene, M., Knox, J.E., Cross, J.B., Bakken, V., Adamo, C., Jaramillo, J., Gomperts, R., Stratmann, R.E., Yazyev, O., Austin, A.J., Cammi, R., Pomelli, C., Ochterski, J.W., Martin, R.L., Morokuma, K., Zakrzewski, V.G., Voth, G.A., Salvador, P., Dannenberg, J.J., Dapprich, S., Daniels, A.D., Farkas, Ö., Foresman, J.B., Ortiz, J.V., Cioslowski, J. and Fox, D.J. Gaussian 09, Revision A.1, Gaussian, Inc., Wallingford CT, 2009.

[17] Becke, A.D. Density-functional exchange-energy approximation with correct asymptotic behavior. *Physical Review A,* 38:3098–3100, 1988.

[18]   Lee, C., Wang, W., and Parr, R.G. Development of the Colle-Salvetti conelation energy formula into a functional of the electron density. *Physical Review B,* 37:785-789, 1988.

[19]   Hay, P.J. and Wadt, W.R. Ab initio effective core potentials for molecular calculations. Potentials for the transition metal atoms Sc to Hg. *Journal of Chemical Physics*, 82:270-283, 1985.

[20]   Hay, P.J. and Wadt, W.R. Ab initio effective core potentials for molecular calculations. Potentials for K to Au including the outermost core orbitals. *Journal of Chemical Physics*, 82:299-310, 1985.

[21]   Gonzalez, C. and Schlegel, H. B. An improved algorithm for reaction path following. *The Journal of Chemical Physics*, 90(4):2154-2161, 1989.

[22]   Joshi, A. M., Tucker, M. H., Delgass, W. N., and Thomson, K. T. CO adsorption on pure and binary-alloy gold clusters: A quantum chemical study. *The Journal of chemical physics*, 125(19):194707, 2006.

[23]   Joshi, A. M., Delgass, W. N. and Thomson, K. T. Analysis of O_2 adsorption on binary-alloy clusters of gold: energetics and correlations. *The Journal of Physical Chemistry B*, 110(46):23373-23387, 2006.

[24]   Wu, D. Y., Ren, B., Jiang, Y. X., Xu, X. and Tian, Z. Q. Density Functional study and normal-mode analysis of the bindings and vibrational frequency shifts of the pyridine-M (M= Cu, Ag, Au, Cu^+, Ag^+, Au^+ and Pt) complexes. *The Journal of Physical Chemistry A*, 106(39):9042-9052, 2002.

[25]   Liu, P., Song, K., Zhang, D. and Liu, C. (2012). A comparative theoretical study of the catalytic activities of Au_2^- and $AuAg^-$ dimers for CO oxidation. *Journal of Molecular Modeling*, 18(5):1809-1818, 2012.

[26]   Getman, R. B. and Schneider, W. F. DFT-based coverage-dependent model of Pt-catalyzed NO oxidation. *ChemCatChem*, 2(11):1450-1460, 2010.

[27]   Tafoughalt, M. A. and Samah, M. Density functional investigation of structural and electronic properties of small bimetallic silver–gold clusters. *Physica B: Condensed Matter*, 407(12):2014-2024, 2012.

[28] Peng, S. L., Gan, L. Y., Tian, R. Y. and Zhao, Y. J. Theoretical study of CO adsorption and oxidation on the gold–palladium bimetal clusters. *Computational and Theoretical Chemistry*, 977(1):62-68, 2011.

[29] Yang, H. Q., Qin, S. and Hu, C. W. Theoretical study on the gas-phase reaction mechanism between nickel monoxide and methane for syngas production. *Journal of Computational Chemistry*, 30(6):847-863, 2009.

[30] Wu, D. Y., Ren, B., Jiang, Y. X., Xu, X. and Tian, Z. Q. (2002). Density Functional Study and Normal-Mode Analysis of the Bindings and Vibrational Frequency Shifts of the Pyridine-M (M= Cu, Ag, Au, Cu+, Ag+, Au+, and Pt) Complexes. *The Journal of Physical Chemistry A*, 106(39):9042-9052, 2002.

[31] Yoneda, T., Takido, T. and Konuma, K. Hydrodechlorination of para-substituted chlorobenzenes over a ruthenium/carbon catalyst. *Applied Catalysis B: Environmental*, 84(3):667-677, 2008.

[32] Fabbi, J. C., Langenberg, J. D., Costello, Q. D., Morse, M. D. and Karlsson, L. Dispersed fluorescence spectroscopy of jet-cooled AgAu and Pt_2. *The Journal of Chemical Physics*, 115(16):7543-7549, 2001.

[33] Huber, K. P. and Herzberg, G. *Constants of diatomic molecules, vol. IV of Molecular Spectra and Molecular Structure*, 1979.

[34] Yoon, B., Häkkinen, H., and Landman, U. Interaction of O_2 with gold clusters: Molecular and dissociative adsorption. *The Journal of Physical Chemistry A*, 107(20):4066-4071, 2003.

[35] Martínez, A. Bonding interactions of metal clusters [M_n (M= Cu, Ag, Au; n= 1-4)] with ammonia. Are the metal clusters adequate as a model of surfaces?. *Journal of the Brazilian Chemical Society*, 16(3A):337-344, 2005.

[36] D. R. Lide, *CRC Handbook of Chemistry and Physics,* Internet Version 2005, http://www.hbcpnetbase.com, CRC Press, Boca Raton, FL, 2005

[37] Lee, T. J. and Taylor, P. R. A diagnostic for determining the quality of single-reference electron correlation methods. *International Journal of Quantum Chemistry*, 36(S23):199-207, 1989.

[38] Miller, S. R., Schultz, N. E., Truhlar, D. G. and Leopold, D. G. A study of the ground and excited states of Al_3 and Al_3^-. II. Computational analysis of the 488 nm anion photoelectron spectrum and a reconsideration of the Al_3 bond dissociation energy. *The Journal of Chemical Physics*, 130(2):024304, 2009.

[39] Häkkinen, H. and Landman, U. Gas-phase catalytic oxidation of CO by Au_2^- *Journal of the American Chemical Society*, 123(39):9704-9705, 2001.

[40] Baishya, S. and Deka, R. C. Catalytic Activities of Au_6, Au_6^-, and Au_6^+ clusters for CO oxidation: A density functional study. *International Journal of Quantum Chemistry*, 114(22):1559-1566, 2014.